RSC Advances

PAPER

View Article Online
View Journal | View Issue

Cite this: *RSC Adv.*, 2020, **10**, 36452

Layered black phosphorus as a reducing agent – decoration with group 10 elements†‡

Jan Plutnar, [a] Zdeněk Sofer [a] and Martin Pumera *[abc]

Received 10th August 2020
Accepted 21st September 2020

DOI: 10.1039/d0ra06884e

rsc.li/rsc-advances

Black phosphorus is prone to surface oxidation under ambient conditions. This attribute is often seen as a negative property of this interesting material. However, its proneness to oxidation – thus the reductive properties – can also be employed in modification of its surface and in preparation of composite materials. Here we describe the process of decoration of BP particles with nickel, palladium and platinum in form of a phosphide or in metallic form, respectively. The deposits have forms of films or nanoparticles and the reported method represents a general way of modifying the surface of black phosphorus with metals or their respective compounds for desired applications.

Introduction

Black phosphorus (BP) belongs to the group of materials rediscovered by material scientists after many decades since their original discovery.[1] Analogous to, for example, graphene, boron nitride, and silicene (and related materials), black phosphorus is a material with a possible future in (sub)micron electronic devices. The structure of the orthogonal BP consists of puckered double-layered sheets of phosphorus atoms arranged into hexagons with 'chair' conformation. Each of the phosphorus atoms in this structure is covalently bound to three adjacent neighbours forming a bond 2.18 Å long. The double-layered sheets are non-covalently stacked, with inter-layer spacing approximately 5 Å.[2] BP is a direct band gap semiconductor (0.3–2.3 eV) with the value of the band gap inversely proportional to the number of the phosphorus double layers in the structure of the material. A material consisting of a single double-layer is commonly known as 'phosphorene' and has the highest value of the band gap,[3] whereas for the bulk material the lowest value of the range was reported. Although BP is the thermodynamically most stable allotrope of phosphorus, it also suffers from an instability towards oxidation by air. This oxidation process can be even faster than the air oxidation of red phosphorus.[4,5] The reason of this behavior can be found in the structure of BP. Arrangement of the phosphorus atoms into the puckered layers results in inevitable orientation of the non-bonding electron pairs above the plane formed by the atoms of the folds of the double layer thus exposing them for a possible reaction. Although an oxidation with oxygen in absence of moisture may result in passivation of the surface, any contact of this layer with water or other protic solvents results in complete deterioration of the material.[6] Much effort was, and still is being made, to surmount the issue of stability of the BP and BP-based materials and devices usually relying on formation of a protective layer of an inert material, *e.g.* aluminum oxide or a polymethyl-methacrylate, thus preventing a contact of BP with the oxidizing environment. However, the reactivity of the surface could also be utilized in its modifications resulting in a change of the properties of the material. This can be achieved *via* formation of either covalent or non-covalent binding interactions with a protective (or substituting) agent.[7–9] The routes of non-covalent modification of BP mostly rely on formation of a relatively strong interaction between the electron-rich surface of BP and an electron-poor guest as reported *e.g.* in modification of BP with 7,7,8,8-tetracyano-*p*-quinodimethane (TCNQ)[10] or with anthraquinone,[11] whereas the covalent modification methods exploit a formation of either P–C or P–O–C bonds.[7–9] Although there were other methods of decoration of the surface of BP reported, they do not exploit the chemical reactivity of the material but rather the structural features of the grooves on the surface of BP to align suitable materials along these wrinkles.[12]

The proneness of BP to oxidation, thus its reductive properties, can also be used in modification of its surface. A brief exposure of a BP sheet to aqueous solution of $HAuCl_4$ results in formation of Au-nanoparticles adhered to the surface of BP.[13,14] Similarly, Ag-nanoparticles can be formed by action of BP

[a]*Center for Advanced Functional Nanorobots, Department of Inorganic Chemistry, University of Chemistry and Technology in Prague Technická 5, Prague 6, 166 28 Czech Republic. E-mail: martin.pumera@vscht.cz; Web: www.twitter.com/PumeraGroup*

[b]*Future Energy and Innovation Laboratory, Central European Institute of Technology, Brno University of Technology, Purkyňova 123, 61200 Brno, Czech Republic*

[c]*Department of Medical Research, China Medical University Hospital, China Medical University, No. 91 Hsueh-Shih Road, Taichung, Taiwan*

† This work was supported by the project Advanced Functional Nanorobots (reg. no. CZ.02.1.01/0.0/0.0/15_003/0000444 financed by the EFRR).

‡ Electronic supplementary information (ESI) available. See DOI: 10.1039/d0ra06884e

nanosheets upon aqueous solution of $AgNO_3$ and 1-dodecylamine.[15] There are also several reports describing an unintended reduction of a metallic precursor to metallic particles, as *e.g.* in the case of the preparation of Co-nanoparticles from an *N*-methylpyrrolidone solution of cobalt(II) acetate at 245 °C[16] or preparation of palladium decorated BP sheets by reduction of $Pd(NO_3)_2$.[17] Oleylamine and gaseous hydrogen were considered as the reducing agents in these reactions, however, BP might play the role of the actual reducing agent here as well. Although these procedures result in inevitable damage to the electronic structure of BP the as-deposited materials can have interesting photocatalytic[15] or electrocatalytic properties.[16]

Leaving aside the electronic properties of BP after such reactions, its reductive properties obviously offer an interesting tool for new preparations of nanomaterials. In addition to the above-mentioned publications – Rosenstein and Donaldson were experimenting with reductive properties of red phosphorus in order to get some insight into its possible use as an agent for qualitative analysis and detection of various elements. In the years 1916–1919, they conducted dozens of experiments involving many compounds, mostly transition metal salts as the reduced species.[18] Inspired also by their work, we had utilized BP as an agent for reduction conjoined with the deposition of the group 10 metals (*i.e.* Ni, Pd, and Pt) or their compounds on its surface *via* reductive formation of either amorphous or crystalline deposits, in form of a layer or separate nanoparticles. These materials were thoroughly studied and possible mechanisms of their formation were suggested.

Results and discussion

Black phosphorus was prepared by a known procedure involving a phosphorus vapor transfer assisted by a presence of SnI_2.[19] The as grown crystals were exfoliated under an inert atmosphere of argon in acetonitrile (MeCN) using shear force milling. The resulting powder was used throughout the experiments as the starting material (BP). Simple salts of the group 10 elements (*i.e.* Ni, Pd, and Pt) were used in the experiments as sources of the metals, namely $NiCl_2 \cdot 6H_2O$, $PdCl_2$, $PtCl_2$, and K_2PtCl_4 and the reactions were done in various solvents (H_2O, MeCN, aq. NH_3) resulting in formation of different morphologies of the metal deposits. The solubility of the salts significantly varies in this series – while $NiCl_2$ is easily soluble in water, $PdCl_2$ and $PtCl_2$ are not. On the other hand, $PdCl_2$ is well soluble in hot MeCN (due to a formation of the $PdCl_2(MeCN)_2$ complex) and could also be dissolved in diluted aqueous HCl (due to the formation of $PdCl_4^{2-}$ anions). Similarly, $PtCl_2$ can be dissolved in aqueous HCl or ammonia solutions. Typically, the reactions were conducted at 70 °C under an inert atmosphere with the molar ratio of BP to the metal 10 : 1. All the materials were characterized by High-Resolution Transmission Electron Microscopy (HRTEM) associated with the Energy-Dispersive X-ray Spectroscopy (EDS) and Selected Area Diffraction (SAD), Raman spectroscopy, X-ray Photoelectron Spectroscopy (XPS) and also an Inductively Coupled Plasma (ICP) analysis in order to assess the chemical composition of the bulk material.

Nickel (BP–Ni)

The reduction of the Ni(II) salt was attempted in deoxygenated water in strongly acidic (aq. HCl), neutral and alkaline (aq. NH_3) solution. Depending on the reaction conditions, the reaction either resulted in a formation of black phosphorus particles completely covered with a nickel-containing layer (in neutral and alkaline solution, Ni-1 and Ni-2 samples, respectively) or no reaction occurred (acidic solution). The ICP analysis results show that the obtained bulk materials consist of 26 wt% of nickel and 70 wt% of phosphorus in the case of the sample Ni-1 and of 35 wt% of nickel and 56 wt% of phosphorus in the case of Ni-2 (the remaining 4 wt% or 9 wt%, respectively, were ascribed to oxygen). The HRTEM analysis of Ni-1 reveals that the layer actually consists of crystalline zones or blended nanoparticles of a size between 8 and 12 nm; the EDS analysis of the particles confirms the presence of nickel evenly spread on their surface (Fig. 1d–f). The polycrystallinity of the nickel layer was also confirmed by the presence of a rich ring-like diffraction pattern visible with the selected area diffraction (SAD) technique (see Fig. 1c). The initial suspicion that this layer consists of a metallic nickel was however not confirmed by the XRD of the material. The diffraction pattern of both materials corresponds to the hexagonal form of dinickel phosphide (Ni_2P, ICDD 74-1385) with characteristic diffraction peaks at 2θ values 40.81, 44.70, 47.41 and 54.33° for Ni-1 and 41.16, 45.00, 47.72 and 54.54° for Ni-2, corresponding to reflections on the (111), (201), (210) and (300) planes, respectively, adhered on the surface of black phosphorus (Fig. 1g and 3g). The (111) reflections were

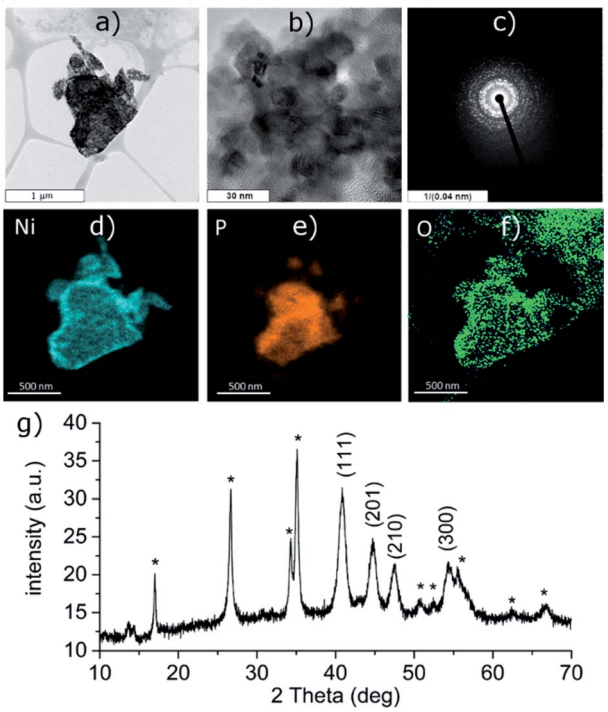

Fig. 1 HRTEM images (a and b), selected area diffraction pattern (c), distribution of the elements (d–f) and the XRD pattern (g) of the Ni-1 composite. Asterisk-labeled peaks represent BP diffractions.

used to approximate the apparent size of the crystalline zones in the materials with the Scherrer equation – $d = \lambda/(K\beta \cos \theta)$ – where d represents the apparent size of a crystallite, λ is the wavelength of the radiation (Cu Kα in our case, $\lambda = 0.15406$ nm), K represents the Scherrer constant (set to 1.0747 as the zones are close to spherical[20]), β is the additional broadening (simplified as a full width of the fitted peak at its half maximum – FWHM) and θ is the Bragg angle in radians. The resulting apparent sizes of the crystalline zones – approximately 10 nm for Ni-1 and 9 nm for Ni-2, respectively – correspond to the results of the HRTEM analyses.

The XPS analysis of the samples also confirms the presence of nickel on the surface of the materials. A deconvolution of the high-resolution spectra of the Ni 2p regions reveals a presence of nickel in two oxidation states (Fig. 2 and S5‡). The lower oxidation state represented by a peak with $E_B = 853.4$ eV corresponds to nickel in Ni_2P. The other signal located at 856.0 or 856.1 eV (in Ni-1 and Ni-2, respectively) was assigned to a Ni(II) species, either a Ni–O from an oxide or hydroxide, or Ni–O–P of the oxidized BP. A deconvolution of the high-resolution spectra of the P 2p regions reveals presence of three peaks at 129.8, 130.7 and 134.4 eV in case of Ni-1 and 129.7, 130.5 and 133.4 eV in case of Ni-2, corresponding to P $2p_{3/2}$, P $2p_{1/2}$ and a mixed signal of the 2p electrons of oxidized phosphorus atoms, respectively (see Fig. 2 and S5‡). The slightly positive shift of the binding energy value of the Ni $2p_{3/2}$ peak together with the slightly negative shift of the P $2p_{3/2}$ peak (when compared with the values of metallic nickel – 852.8 eV – and black phosphorus – 130.3 eV, respectively) indicate a partial positive charge on Ni and partial negative charge on P in Ni_2P. Because of the thickness of the Ni_2P layer, no signals corresponding to BP were identified on the XPS spectra of the samples. On the other hand, the Raman spectra of the materials show the common features of BP materials, with the energies of the main vibration modes slightly shifted when compared to those of the pristine black phosphorus,[21] namely the B_{1g}, B_{3g}, A_g^1, B_{2g} and A_g^2 modes with energies at 192.0, 227.0, 359.1, 434.3 and 461.6 cm^{-1}, and 194.2, 229.4, 361.7, 438.3 and 466.6 cm^{-1} for Ni-1 and Ni-2, respectively (Fig. S9 and S10‡).

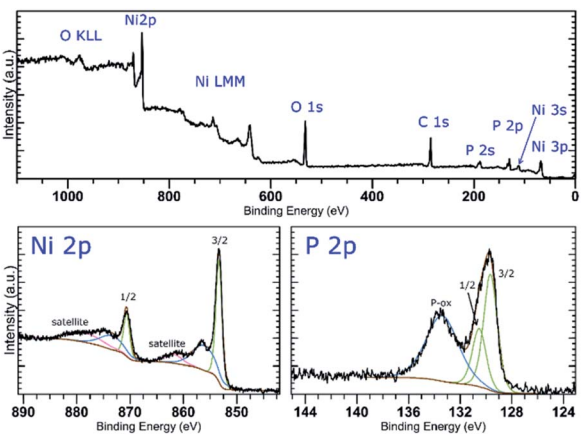

Fig. 2 XPS survey spectrum (top) and high-resolution spectra of the Ni 2p and P 2p regions (bottom) of Ni-2.

Palladium (BP–Pd)

$PdCl_2$ was used as a precursor for preparation of palladium-decorated black phosphorus particles; the morphology and composition of the particles were dependent on the solvent and reaction conditions used for the preparation of the material. Whereas the reaction of the Pd(II) salt in acetonitrile resulted in a formation of BP particles completely covered with an amorphous palladium layer (Pd-1), the reaction of an acidic aqueous solution of the Pd(II) salt resulted in a formation of BP particles decorated with discrete crystalline palladium nanoparticles (Pd-2). A reaction in concentrated aqueous ammonia resulted in deposition of palladium nanoparticles on the surface of BP in some cases (Pd-3), according to the XRD analysis is the majority of the deposited palladium amorphous. The ICP analysis shows that the materials contain 47 wt%, 61 wt%, and 55 wt% of palladium and 46 wt%, 35 wt%, and 35 wt% of phosphorus (for Pd-1, Pd-2, and Pd-3, respectively) with 7, 4, and 10 wt% assigned to oxygen. XRD analysis of the materials revealed the amorphous character of Pd-1 as only the diffraction peaks corresponding to BP were observed being overlapped by the characteristic peak of an amorphous material (Fig. S2‡). On the other hand, the peaks corresponding to a presence of crystalline metallic palladium were identified in the XRD pattern of Pd-2. The diffraction patterns correspond to the face centered cubic structure of palladium (ICDD 87-0641) with characteristic diffraction peaks at 2θ values 40.25, 46.80, 68.26, 82.22 and 86.75°, corresponding to reflections on the (111), (200), (220), (311) and (222) planes, respectively, adhered onto the surface of BP (Fig. 3). The XRD pattern of Pd-3 suggests the material consists of a majority of an amorphous palladium deposit with

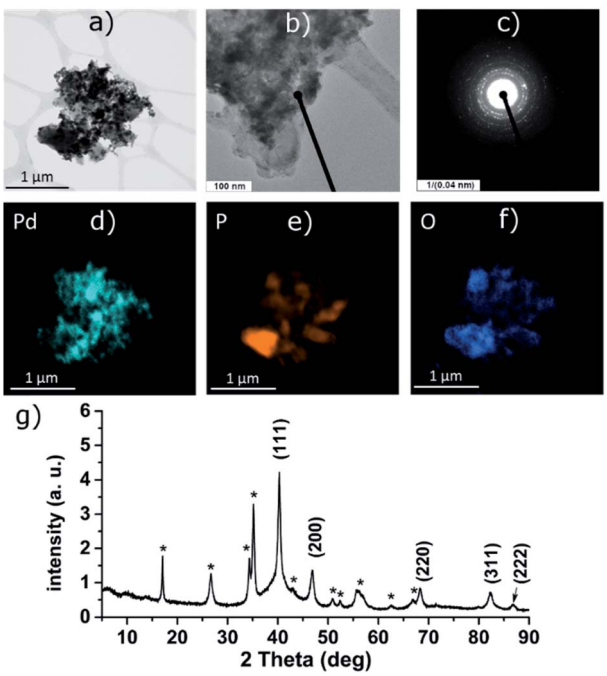

Fig. 3 HRTEM images (a and b), selected area diffraction pattern (c), distribution of the elements (d–f) and the XRD pattern (g) of Pd-2. Asterisk-labeled peaks represent BP diffractions.

hardly distinguishable peaks at 40.4 and 47.0° corresponding to diffractions along the (111) and (200) planes. The HRTEM and EDS analyses of Pd-1 reveal an almost homogeneous coverage of the BP particles with palladium (Fig. S2‡). In the case of Pd-2, clearly distinguishable particles of a size 10–16 nm are visible (Fig. 3). The HRTEM analysis of Pd-3 reveals presence of some BP particles almost homogeneously covered with Pd together with few decorated with discrete crystalline Pd nanoparticles (Fig. S3‡). As already mentioned, the XRD indicates the prevailing presence of the amorphous palladium layer. An analysis of the XRD data of Pd-2, using the (111) diffraction peak and the Scherrer equation, reveals an apparent particle size 14 nm. The XPS analysis of all samples does not show much difference in the composition of valence states of palladium. A deconvolution of the high-resolution spectra of the Pd 3d region reveals the presence of majority of palladium in zerovalent state in all the samples (81, 83, and 96% for Pd-1, Pd-2, and Pd-3, respectively) with binding energy Pd $3d_{5/2}$ peaks at 335.0 eV (Fig. 4, S6 and S7‡).

The other Pd state represents only a minor component of the Pd 3d signal in all cases, with the Pd $3d_{5/2}$ binding energy peaks at 336.4, 336.7 and 337.5 eV (for Pd-1, Pd-2, and Pd-3, respectively). The value of the binding energy observed for the higher valence state of palladium, although attributable to Pd(II), also well corresponds to the values of Pd(0) in coordination compounds in which the palladium central atom is surrounded solely by phosphorus atoms (*e.g.* $[Pd(PPh_3)_4]$ or $[Pd_2(PPh_3)_2]$).[22] We presume that the electrons of these binding energies are being emitted from the palladium atoms located in the areas of the Pd layer or the Pd particles which are in direct contact with the phosphorus atoms. An overlap of the valence orbitals of these palladium atoms and BP might cause an electron redistribution in the affected Pd(0) atoms resulting in the observed shift in the binding energies of the Pd 3d electrons.[17,23] On the other hand, the composition of the valence states of phosphorus significantly differs amongst the samples. A deconvolution of the high-resolution spectra of P 2p regions reveals a presence of peaks at 129.8 and 130.7 eV corresponding to the $2p_{3/2}$ and $2p_{1/2}$ spin orbit peaks together with a broad peak corresponding to phosphorus in higher oxidation states in all the samples (Fig. 4, S6 and S7‡). While in the case of the amorphous sample Pd-1 the material contains approximately 64% of phosphorus in a higher oxidation state (P 2p $E_B = 134.6$ eV), the crystalline sample Pd-2 contains only approximately 30% of the same (P 2p $E_B = 134.4$ eV), and the mixed morphology sample Pd-3 also contains approximately 34% of the higher oxidation state phosphorus (P 2p $E_B = 134.4$ eV). In addition to these two main signals an additional pair of peaks can be identified in the deconvoluted data of both samples that could be assigned to phosphorus coordinated to palladium.[17,22] The $2p_{3/2}$ peaks were identified at 131.2 eV and 130.9 eV in Pd-1 and Pd-2, respectively. In the case of Pd-3 is the amount of the Pd-coordinated phosphorus very small (approximately 4% according to the analysis of the Pd 3d core line XPS spectrum) and we were not able to properly fit the respective signals in the P 2p spectrum of the sample. Analogously to the nickel-containing sample, the Raman spectra of all three materials show the common features of a BP material. The energies of the B_{1g}, B_{3g}, A_g^1, B_{2g} and A_g^2 vibration modes are located at 194.2, 229.5, 361.8, 437.9 and 466.4 cm^{-1}, respectively, for Pd-1 (Fig. S11‡) and at 193.4, 228.5, 360.4, 436.4 and 465.0 cm^{-1}, respectively, for Pd-2 (Fig. S12‡) and 194.2, 229.4, 361.7, 438.3 and 466.6 cm^{-1}, respectively, for Pd-3 (Fig. S13‡).

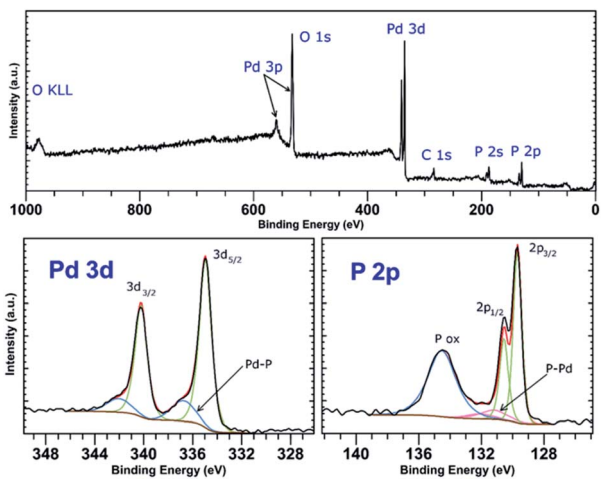

Fig. 4 Survey XPS spectrum (top) and high-resolution spectra of the Pd 4d and P 2p regions (bottom) of Pd-2.

Platinum (BP–Pt)

$PtCl_2$ and K_2PtCl_4 were used as the precursors for preparations of the platinum-decorated BP. As $PtCl_2$ is neither soluble in any organic solvent or in water, concentrated aqueous ammonia was used to dissolve it *via* formation of the tetraammineplatinum(II) chloride complex. In both cases, platinum nanoparticles were deposited on the surface of BP. The ICP analysis shows the content of platinum is approximately 32 and 38 wt% in Pt-1 and Pt-2, respectively. At the same time, the content of phosphorus was 59 and 52 wt% in the same respective samples, leaving approximately 9 and 10 wt% of the material to oxygen. XRD analyses of both samples revealed crystallinity of the deposited material on the surface of BP. In both cases the material deposited on BP consists of face centered cubic phase of platinum (ICDD 04-0802) deposited over the BP particles. The main diffraction peaks corresponding to the diffractions along the (111), (200), (220), (311) and (222) planes were found at 2θ values 40.12, 46.60, 67.86, 81.74 and 86.15°, respectively, for Pt-1 (Fig. S4g‡) and at 2θ values 40.06, 46.43, 67.74, 81.63 and 86.18°, respectively, for Pt-2 (Fig. 5g). The HRTEM analysis of the materials confirms the presence of the nanoparticles on the surface of the BP particles in both cases and the EDS analysis showed that these particles actually consist of platinum (Fig. S4a–f‡ for Pt-1 and Fig. 5a–f for Pt-2). The SAD patterns confirm the crystallinity of the particles. The average size of the nanoparticles was determined by the analysis of the HRTEM images and approximated from the XRD data according to the Scherrer with (111) diffraction peaks used for the approximation resulting in the apparent size of the metallic nanoparticles

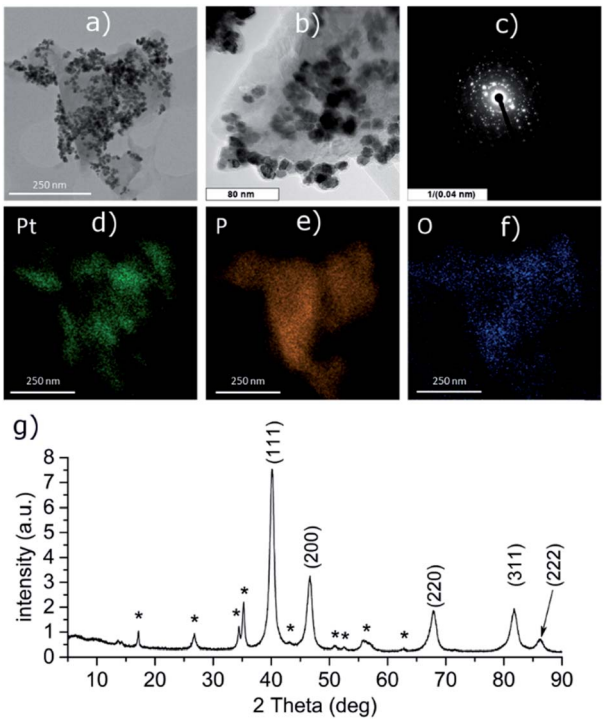

Fig. 5 HRTEM images (a and b), selected area diffraction pattern (c), distribution of the elements (d–f) and the XRD pattern (g) of Pt-2. Asterisk-labeled peaks represent BP diffractions.

approximately 10 nm in Pt-1 and approximately 6 nm in Pt-2. These values well correspond to the size of the particles determined by the analysis of the HRTEM images (approximately 11 nm for the former and 5 nm for the latter one, respectively). The HRTEM images also reveal, that in the case of Pt-1 are the particles aggregated into larger 'clusters' of platinum (of a size around 250 nm), while in the case of Pt-2 the particles are more evenly spread on the surface of the BP particles. A deconvolution of the high-resolution spectra of the Pt 4f region of the XPS spectra of both samples revealed a presence of platinum in two valence states (Fig. 6 and S8‡). The majority of both samples (72 and 89%, respectively) is represented by platinum in zerovalent state as indicated by a presence of peaks with Pt $4f_{7/2}$ $E_B = 70.7$ and 70.6 eV for the Pt-1 and Pt-2, respectively. We presume, that similarly to the Pd samples, the signals corresponding to a higher valence state of the platinum atoms (with $4f_{7/2}$ E_B = 72.3 and 72.6 eV, respectively) belong to the atoms of the outer shells of the particles that are in direct contact with the phosphorus atoms. The high-resolution spectra of the 2p core level of phosphorus reveal presence of almost 31% and 48% of BP being oxidized in Pt-1 and Pt-2, respectively, as indicated by a presence of signals with $E_B = 134.0$ and 133.7 eV, respectively. In addition, the peaks corresponding to the $2p_{3/2}$ and $2p_{1/2}$ spin orbit components of black phosphorus in both samples were identified at 129.7 and 130.6 eV, respectively. As in the case of the palladium-containing materials, additional signals were identified in the deconvoluted spectra. The $2p_{3/2}$ peaks were found at 130.8 and 130.7 eV in Pt-1 and Pt-2, respectively. Also, these signals were assigned to phosphorus atoms coordinated

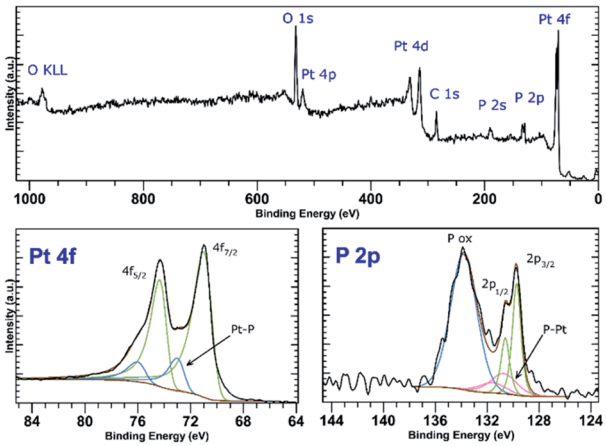

Fig. 6 Survey XPS spectrum (top) and high-resolution spectra of the Pt 4f and P 2p regions (bottom) of Pt-2.

to platinum. Analogously to the previous materials, the Raman spectra of Pt-1 as well as of Pt-2 exhibit the common features of a BP material. The energies of the B_{1g}, B_{3g}, A_g^1, B_{2g} and A_g^2 vibration modes are located at 192.8, 228.3, 359.2, 434.3 and 462.2 cm^{-1}, respectively, for Pt-1 (Fig. S14‡) and at 193.5, 229.6, 361.2, 437.7 and 465.3 cm^{-1}, respectively, for Pt-2 (Fig. S15‡).

Several different materials containing nickel, palladium and platinum, either in a form of a binary compound (Ni_2P) or in a metallic form were deposited on the surface of BP particles (Table 1) utilizing a redox reaction in which the BP plays a role of the reducing agent. On the contrary to the reported methods of preparation of Ni_2P deposited on black phosphorus, comprising of high temperature annealing of metallic nickel electrodes touching the surface of BP[24] or a nickel(II)-doped surface of BP in the presence of tri-*n*-octylphosphine,[25] our method consists of a simple low-temperature treatment of a BP/Ni(II) salt mixture in water or in aqueous ammonia using even milder conditions than in the reported preparation of Ni_2P nanoparticles using red phosphorus as the reducing agent and the phosphide precursor at the same time.[26] The morphology of the obtained materials could be described as a continuous film of the Ni/P alloy with randomly oriented crystalline domains of the hexagonal Ni_2P rather than an agglomerate of regular nanoparticles. We hesitate to speculate excessively about the mechanism of the Ni_2P formation but we presume that the overall progress of the process could be expressed by eqn (1).

$$2Ni^{2+} + P_x + 4H_2O \rightarrow Ni_2P + 4H^+ + P_{(x-1)}(OH)_4 \quad (1)$$

In this reaction, Ni^{2+} represents both, $[Ni(H_2O)_6]^{2+}$ in the neutral aqueous solution as well as $[Ni(NH_3)_6]^{2+}$ in the aqueous ammonia. BP here formally acts as both, the reducing and the reduced species. In the progress of the reaction, the oxidized BP slowly dissolves in water[6] or aqueous ammonia as confirmed by a relatively low intensity of the signal corresponding to the higher oxidation states of phosphorus in the XPS spectra of the materials. ^{31}P NMR spectroscopy of the mother liquors

Table 1 Summary of reaction conditions and properties of the products

Metal	Precursor	pH	Solvent	T [°C]	Product	Appearance	Label
Ni	$NiCl_2 \cdot 6H_2O$	Neutral	Water	70	Ni_2P	Continuous layer, crystalline	**Ni-1**
Ni	$NiCl_2 \cdot 6H_2O$	Acidic	Water	70	Ni_2P	Continuous layer, crystalline	**Ni-2**
Pd	$PdCl_2$	—	Acetonitrile	70	Pd	Continuous layer, amorphous	**Pd-1**
Pd	$PdCl_2$	Acidic	Water	70	Pd	Discrete nanoparticles (∼14 nm), crystalline	**Pd-2**
Pd	$PdCl_2$	Basic (NH_3)	Water	70	Pd	Mixed amorphous–crystalline	**Pd-3**
Pt	K_2PtCl_4	Neutral	Water	70	Pt	Aggregated nanoparticles (∼10 nm), crystalline	**Pt-1**
Pt	$PtCl_2$	Basic (NH_3)	Water	70	Pt	Discrete nanoparticles (∼6 nm), crystalline	**Pt-2**

confirmed the presence of phosphorus in phosphates and phosphites (Fig. S16‡). Presumably, the overall mechanism of the reaction resembles the processes involved in the hypophosphite-based electroless nickel-coating process,[27] although in this case the phosphide represents the major product of the reaction.

Surprisingly, no reaction between the solution of the nickel(II) salt and BP in strongly acidic medium (1 M aq. HCl) occurred. The XPS spectrum of the material isolated after the reaction reveals only a hardly detectable contamination of BP with nickel (Fig. S17‡). Also, no oxidation of BP is detected. Although we have no direct confirmation of the following explanation, we presume that a synergy of the possible repulsion of the negatively charged $NiCl_4^{2-}$ ions by the partially negatively charged surface of the partially oxidized BP surface and the relatively lower difference between the redox potentials of the Ni^{2+} to $Ni^{\delta+}$ reduction and P(0) to P(III) and P(V) oxidations in acidic than in basic solutions is the key.[28]

In the case of palladium, three reactions under different conditions were tested, all of them using palladium(II) chloride as the source of palladium. Due to the limited solubility of $PdCl_2$ in water, acetonitrile was chosen as the solvent for the first experiment. Upon dissolution of the chloride, $[Pd(MeCN)_4]^{2+}$ complex is initially formed, which subsequently reacts with BP. Amorphous palladium layer is formed as the result of this reaction (Pd-1). In the second experiment, $PdCl_2$ was dissolved in a diluted solution of hydrochloric acid thus resulting in formation of the $PdCl_4^{2-}$ anion. The subsequent reaction with BP resulted in discoloration of the initially orange-yellow solution and formation of crystalline Pd nanoparticles on the surface of the BP (Pd-2). In the third reaction, $PdCl_2$ was dissolved in concentrated aqueous ammonia thus forming the $Pd(NH_3)_4^{2+}$ cation solution. The mechanism of the metallic palladium formation remains unclear in the case of formation of the amorphous material, however, as we presume that the reaction in acidic water might proceed according to the eqn (2), a similar mechanism (involving a presence of traces of water in the reaction media) might be found behind the formation of Pd-1 as well. The presence of some source of oxygen is evident from the XPS spectra of the Pd-1 sample. We presume that some moisture might be present in the solvent. On the other hand, the amount of the such introduced water was most likely small as it was not sufficient to dissolve the oxidized BP layer in Pd-1, on the contrary to the relatively low amount of oxygen (or indirectly, the phosphorus in higher oxidation states) detected in the XPS spectra of the Pd-2 and Pd-3 samples prepared in acidic or ammonia water (55.6 *vs.* 34.8 and 34.0 at%, respectively) which presumably results from dissolution of the oxidized surface in water (as confirmed by NMR, see below).

$$[MCl_4]^{2-} + 2H_2O + P_x \rightarrow M(s) + 2Cl^- + 2HCl + P_x(OH)_2 \quad (2)$$

Similarly, the reaction of $Pd(NH_3)_4^{2+}$ could follow the reaction suggested in eqn (3) below.

$$[M(NH_3)_4]^{2+} + 2H_2O + P_x \rightarrow M(s) + 2NH_4^+ + 2NH_3 + P_x(OH)_2 \quad (3)$$

In the above-mentioned reactions, M represents either palladium or platinum. On the contrary to nickel, the value of the pH of the solution (or in other words, the charge of the complex ion) wasn't the decisive property in the redox process as in all cases elemental palladium was formed. Similarly to Ni, both P(III) and P(V) oxidation products were detected in mother liquors of the chemical reactions by NMR. Besides the phosphite and phosphate anions, also some orthophosphate was detected (Fig. S18‡).

Reduction of $PtCl_2$ dissolved either in diluted HCl or in concentrated aqueous NH_3 solutions with BP resulted in a formation of crystalline platinum nanoparticles in both cases. A reduction of the *in situ* formed $[Pt(NH_3)_4]^{2+}$ complex yielded crystalline nanoparticles only negligibly larger than those prepared by an analogous reduction of the *in situ* formed $PtCl_4^{2-}$ complex. The nanoparticles in the former material (Pt-1) aggregate to form 250 nm large clusters whereas the nanoparticles in the latter material (Pt-2) are spread over the surface of the BP particles without any apparent clustering. The mechanism of the $PtCl_4^{2-}$ reduction is most likely identical to the one of the palladium analogues described by the eqn (2). Similarly, the reductive process of formation of platinum in ammonia is analogous to eqn (3).

Conclusion

As shown in the preceding text, black phosphorus can be successfully used as a reducing agent for production of various

materials containing group 10 elements. In some cases (Ni, Pd), BP particles covered by a continuous layer of the produced material (Ni_2P or Pd) are prepared under the given reaction conditions. Under some reaction conditions, BP covered with discrete metallic particles (Pd, Pt) as nanoparticles or their aggregates can be obtained. Interestingly, the reaction of BP with Ni(II) salt under relatively mild conditions resulted in formation of Ni_2P instead of metallic nickel film or nickel particles. The procedure of Ni_2P preparation described herein offers an alternative route towards preparation of this promising hydrogen evolution catalytic system. Although the presented data suggest an inevitable damage to the surface of the BP particles as the result of the redox reaction, the as prepared Pt and Pd–BP composites possess interesting structural features and could possibly serve *e.g.* as catalysts in various chemical processes where the presence of platinum group metals is required, taking advantage of the BP carrier as a "green" (in terms of the oxidative degradability to phosphates) material on one side and the possibility of their relatively simple *in situ* preparation (if desired) on the other. The above-described results also confirm, that in many of the already mentioned procedures black phosphorus (intended as a substrate or carrier of another material) also acted as the actual reducing agent instead of the added reducing agent (hydrogen[17] *etc.*).

Conflicts of interest

There are no conflicts to declare.

Acknowledgements

This work was supported by the project Advanced Functional Nanorobots (Reg. No. CZ.02.1.01/0.0/0.0/15_003/0000444 financed by the EFRR).

References

1 P. W. Bridgman, *J. Am. Chem. Soc.*, 1914, **36**, 1344–1363.
2 A. Brown and S. Rundqvist, *Acta Crystallogr.*, 1965, **19**, 684–685.
3 Z. Guo, H. Zhang, S. Lu, Z. Wang, S. Tang, J. Shao, Z. Sun, H. Xie, H. Wang, X.-F. Yu, *et al.*, *Adv. Funct. Mater.*, 2015, **25**, 6996–7002.
4 M. R. Somayajulu, G. K. Gautam and A. S. Rao, *Def. Sci. J.*, 2007, **57**, 817–824.
5 Y. Abate, D. Akinwande, S. Gamage, H. Wang, M. Snure, N. Poudel and S. B. Cronin, *Adv. Mater.*, 2018, **30**, 1704749.
6 J. Plutnar, Z. Sofer and M. Pumera, *ACS Nano*, 2018, **12**, 8390–8396.
7 C. R. Ryder, J. D. Wood, S. A. Wells, Y. Yang, D. Jariwala, T. J. Marks, G. C. Schatz and M. C. Hersam, *Nat. Chem.*, 2016, **8**, 597–602.
8 Z. Sofer, J. Luxa, D. Bouša, D. Sedmidubský, P. Lazar, T. Hartman, H. Hardtdegen and M. Pumera, *Angew. Chem., Int. Ed.*, 2017, **56**, 9891–9896.
9 M. van Druenen, F. Davitt, T. Collins, C. Glynn, C. O'Dwyer, J. D. Holmes and G. Collins, *Chem. Mater.*, 2018, **30**, 4667–4674.
10 G. Abellán, V. Lloret, U. Mundloch, M. Marcia, C. Neiss, A. Görling, M. Varela, F. Hauke and A. Hirsch, *Angew. Chem., Int. Ed.*, 2016, **55**, 14557–14562.
11 R. Gusmão, Z. Sofer and M. Pumera, *ACS Nano*, 2018, **12**, 5666–5673.
12 D. W. Kim, H. S. Jeong, K. O. Kwon, J. M. Ok, S. M. Kim and H.-T. Jung, *Adv. Mater. Interfaces*, 2016, **3**, 1600534.
13 H. Huang, Q. Xiao, J. Wang, X.-F. Yu, H. Wang, H. Zhang and P. K. Chu, *npj 2D Mater. Appl.*, 2017, **1**, 20.
14 Q. Wu, M. Liang, S. Zhang, X. Liu and F. Wang, *Nanoscale*, 2018, **10**, 10428–10435.
15 X. Wang, B. Zhou, Y. Zhang, L. Liu, J. Song, R. Hu and J. Qu, *J. Alloys Compd.*, 2018, **769**, 316–324.
16 F. Shi, Z. Geng, K. Huang, Q. Liang, Y. Zhang, Y. Sun, J. Cao and S. Feng, *Adv. Sci.*, 2018, **5**, 1800575.
17 M. Vanni, M. Serrano-Ruiz, F. Telesio, S. Heun, M. Banchelli, P. Matteini, A. M. Mio, G. Nicotra, C. Spinella, S. Caporali, *et al.*, *Chem. Mater.*, 2019, **31**, 5075–5080.
18 L. Rosenstein, *J. Am. Chem. Soc.*, 1920, **42**, 883–889.
19 M. Köpf, N. Eckstein, D. Pfister, C. Grotz, I. Krüger, M. Greiwe, T. Hansen, H. Kohlmann and T. Nilges, *J. Cryst. Growth*, 2014, **405**, 6–10.
20 J. I. Langford and A. J. C. Wilson, *J. Appl. Crystallogr.*, 1978, **11**, 102–113.
21 S. Sugai and I. Shirotani, *Solid State Commun.*, 1985, **53**, 753–755.
22 *NIST X-ray Photoelectron Spectroscopy Database, NIST Standard Reference Database Number 20*, National Institute of Standards and Technology, Gaithersburg MD, 20899 (2000), (retrieved [15.02.2020]).
23 M. Caporali, A. Guerriero, A. Ienco, S. Caporali, M. Peruzzini and L. Gonsalvi, *ChemCatChem*, 2013, **5**, 2517–2526.
24 Z.-P. Ling, S. Sakar, S. Mathew, J.-T. Zhu, K. Gopinadhan, T. Venkatesan and K.-W. Ang, *Sci. Rep.*, 2015, **5**, 1–8.
25 Y. Lin, Y. Pan and J. Zhang, *Int. J. Hydrogen Energy*, 2017, **42**, 7951–7956.
26 Y. Deng, Y. Zhou, Y. Yao and J. Wang, *New J. Chem.*, 2013, **37**, 4083–4088.
27 J.-P. Randin and H. E. Hintermann, *J. Electrochem. Soc.*, 1968, **115**, 480–484.
28 S. G. Bratsch, *J. Phys. Chem. Ref. Data*, 1989, **18**, 1–21.

